Tunable V-Cavity Laser with Butt-Joint Passive Tuning Section for Fast Wavelength Switching

Xiaolu Liao
Jia Guo
Jian-Jun He, *Senior Member, IEEE*
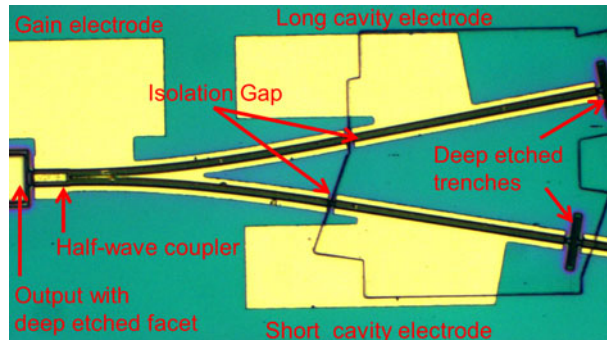
Tunable V-Cavity Laser with Butt-Joint Passive Tuning Section for Fast Wavelength Switching

Xiaolu Liao, Jia Guo, and Jian-Jun He, *Senior Member, IEEE*

State Key Laboratory of Modern Optical Instrumentation, College of Optical Science and
Engineering, Zhejiang University, Hangzhou 310027, China

Abstract: We report on the fast carrier-induced wavelength switching in V-cavity laser using butt-joint passive tuning section. Using the carrier plasma based tuning effect in combination with temperature induced gain spectrum shift, over 25-nm wavelength tuning with 100 GHz channel spacing is obtained with side-mode suppression ratio up to 40 dB. Sixteen channels can be switched by using a single electrode control on the long cavity electrode and seven channels on the short cavity electrode. Mode competition is observed during the transient and the switching delay time varies from 1 to 11 ns for different switching paths.

Index Terms: Semiconductor laser, V-cavity laser, tunable laser.

1. Introduction

The wavelength division multiplexing passive optical networks (WDM-PONs) is a promising way to greatly increase the capacity of optical access networks [1], [2]. Colorless transmitters or port-agnostic tunable transceiver are highly desirable for optical network units (ONUs) so that the costs of the system installation and maintenance can be reduced dramatically. V-cavity laser (VCL) are good candidates for such applications due to its compactness, fabrication simplicity and simple electronic driver [3], [4]. Compared with the sampled grating (SG) DBR lasers [5], the VCL has a very small size, simple wavelength control algorithm, and does not involve any grating. Besides, it is easier to be calibrated due to the fact that only one electrode is to be controlled making it more time saving and suitable for mass production. Also compared with the three section DBR lasers which are limited to 10 nm tuning [6], the V-cavity laser is capable of full C band wavelength tuning [7]. However, most of the previously demonstrated VCL employed all-active layer structure for simple fabrication. The tuning mechanism is based on current induced thermal-optic effect, which requires a high tuning current up to 140 mA, and the tuning speed is slow ($\sim$20 μs) [7]. By applying the carrier-induced wavelength tuning, the driving current of VCL can be reduced, and the wavelength switching time is reduce to nanosecond level by using passive tuning sections based on quantum well intermixing (QWI) technology [8]. Since the bandgap shift by QWI is limited, the residual absorption in the intermixed QW waveguide is usually high, which limits the sizes of the passive device sections. Another promising solution for active-passive integration is butt-joint waveguide [9]
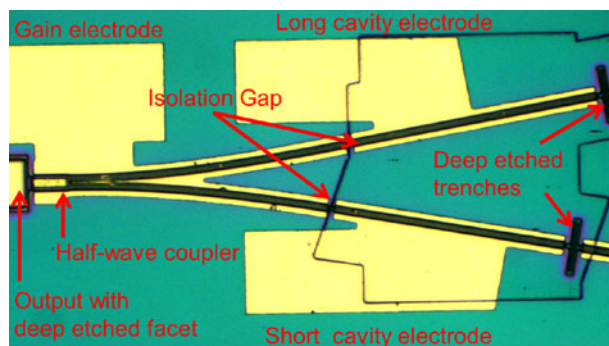
Fig. 1. Schematic structure of the VCL.

which allows fast switching as well as low propagation loss in the passive waveguides and thus the integration of large passive devices such as wavelength multiplexers.

In this paper, we report the first experimental results of carrier-injected wavelength tuning in VCL with butt-jointed passive tuning section. At a fixed temperature, single-electrode-controlled consecutive wavelength tuning of 16 channels was demonstrated with side-mode suppression ratio up to 41 dB. Further a 32-channel tuning of 100 GHz spacing is demonstrated by combining temperature-induced gain spectrum shift with a temperature variation of only 28 °C. Since the carrier plasma effect is particularly important for realizing fast switching, the wavelength switching time of turn-on and turn-off between different channels are investigated.

2. Device Structure and Fabrication

The layers were grown by metal-organic vapor phase epitaxy (MOVPE) in a three-step process. In the first epitaxy step, the active section with a 1% compressive strained laser structure containing five InGaAsP QWs sandwiched by InGaAsP step-graded index confining layers are grown [7]. Passive area blocks are defined by photolithography using a 1 μm SiO$_2$ layer as etching mask and they are etched wet chemically 30 nm below the active layer for regrowth. Then the passive layer stacked with quaternary layer ($\lambda_g = 1.25$ μm) with a thickness of 350 nm are regrown afterwards by selective area MOVPE using the same SiO$_2$ mask. The mask is removed and a p-doped top cladding layer is grown.

Standard fabrication process for ridge waveguide Fabry-Perot lasers was executed with the addition of a deep-etching step for the etched facets [10]. The top-view photograph of the VCL is given in Fig. 1. It consists of two Fabry–Perot cavities with slightly different lengths and a reflective 2 × 2 half-wave coupler [11]. The two coupled cavities are defined by deep etched facets and deep etched trenches. The length of the short cavity is designed to be 432 μm so that its resonant wavelength matches the ITU grids of 100 GHz spacing and the other cavity is 6.5% longer so that the wavelength tuning range is magnified by the Vernier effect. The waveguides under the long and short cavity electrodes are processed to be passive waveguides using the butt-joint technology. In operation, a fixed current is applied to the gain electrode. The tuning current on the long cavity electrode changes the effective refractive index of the waveguide to tune the wavelength of the laser. Theoretically, the tuning range is limited by the free spectral range (FSR) of about 16 channels considering of the length difference between the two cavities of 6.5% [15]. The length ratios between the passive and active sections are designed to be the same in the two cavities so that no mode hop occurs when increasing the injection current on the gain electrode, which is very important for direct intensity modulation. The chip size is only about 500 μm × 250 μm.

According to the threshold condition of the VCL in [4], the threshold gain difference between the lowest threshold mode and the next lowest threshold mode, and the corresponding side-mode suppression ratio (SMSR) as a function of the normalized bar-coupling coefficient C$_{11}$ are shown in
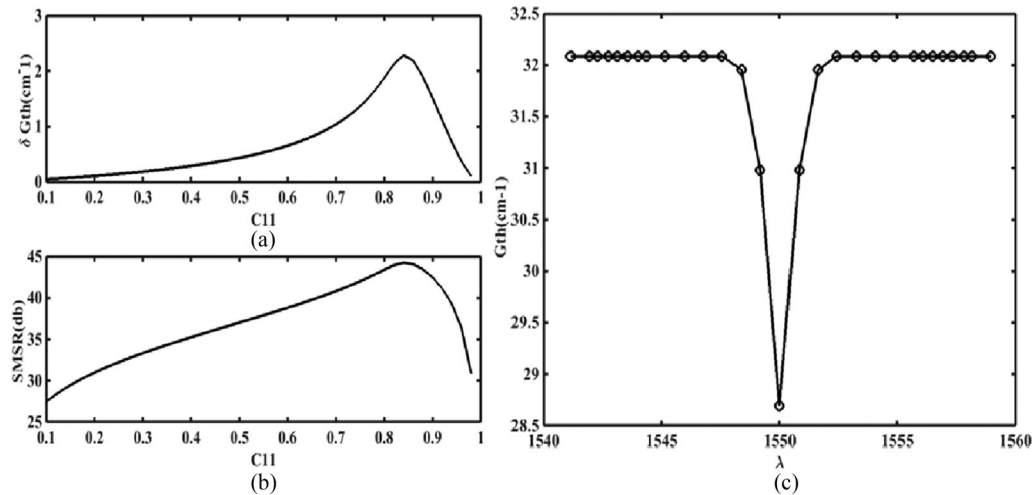
Fig. 2. (a) Threshold gain difference between the lowest threshold mode and the next lowest threshold mode and (b) the corresponding side-mode suppression ratio as a function of the normalized bar-coupling coefficient C_{11}, and (c) the threshold gain for all longitudinal modes.
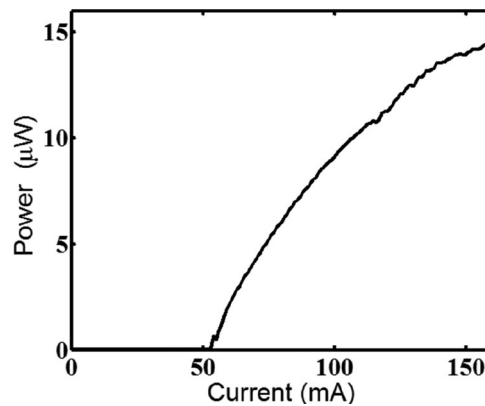

Fig. 3. Measured output power as a function of injected current on the gain electrode.

Fig. 2 (a) and (b). We can see that the largest threshold difference occurs around $C_{11} = 0.84$ and the SMSR can reach as high as 45 dB according to the simple model of [12] without considering the spatial hole-burning effect. The corresponding threshold gain for all longitudinal modes is shown in Fig. 2(c). Finally after the BPM simulation for half-wave coupler, the gap, the width and length of the multimode section are determined to be 3.1 μm, 10.1 μm and 29.5 μm, respectively.

3. Device Characterizations and Discussion

The chip is mounted on an AlN heat sink for the device characterization. For wavelength tuning and switch characterization, the light from the deep etched facet of the device is coupled into a single mode fiber using 3-Axis NanoMax Flexure Stages and measured by an optical spectrum analyzer (OSA).

Fig. 3 plots the light output power collected by a fiber-coupled detector from the coupler side as function of the gain current at 15 °C with the long and short cavity section unbiased. The etched facet on the coupler side is coated with a 30 nm Au to increase the reflectivity. The measured power is therefore low and is only indicative for relative power monitoring. It can be seen that the threshold
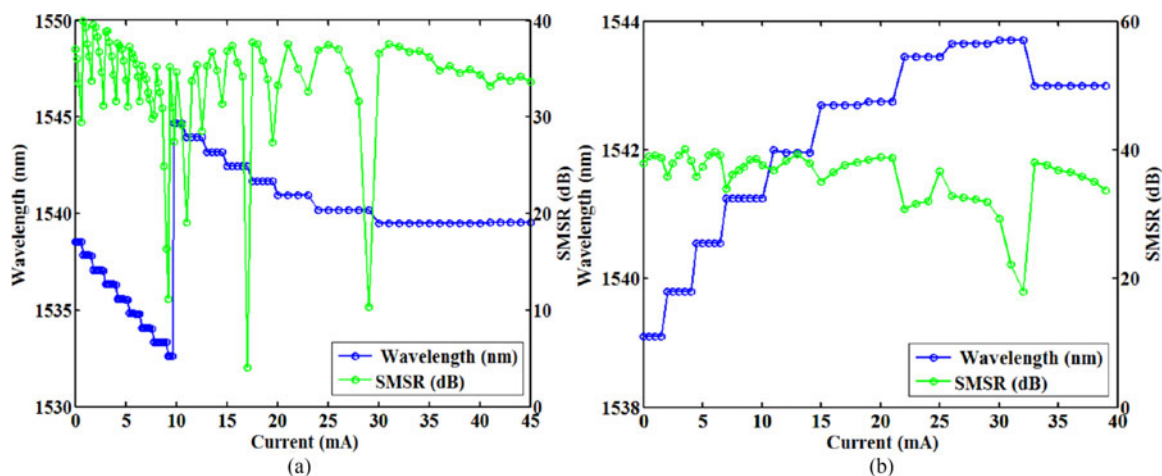
Fig. 4. (a) Typical measured wavelength and SMSR characteristics of the V-cavity laser during the tuning of the long cavity electrode and (b) the short cavity electrode.

current of the device is about 53 mA, a little higher than those of previously reported VCL [13]. This can be explained by two reasons. Firstly, the fabrication in this first run of butt-joint passive-active integrated VCL is non-ideal, which causes high internal loss. Besides, the passive section occupies 45% of the whole FP cavity, compared to 30% in [13]. Secondly, the actual widths of the deeply etched trenches are deviated from the ideal value of $3\lambda/4$ for high reflectivity. A deviation of 300 nm will decrease the reflectivity of the trenches from 70% to 30%. Here we mainly demonstrate the carrier-induced tuning effect by butt-joint technology to achieve the fast switching. The propagation loss of the passive waveguide needs to be improved in future work.

To investigate the single electrode-controlled tuning characteristics of the V-cavity laser, the gain electrode and the short cavity electrode are biased at 150 and 0 mA, respectively, and the injection current on the long cavity electrode is varied from 0 to 45 mA. As the short cavity was processed to be passive section, no current was needed on this electrode. As shown in Fig. 4(a), we can see that wavelength tuning of 16 consecutive channels with 100 GHz channel spacing from 1534.6 to 1546.75 nm is achieved, which is consistent with the design. Fig. 4(b) shows the peak wavelength of the VCL when the short cavity current was varied from 0 to 40 mA while no current is injected in the long cavity electrode. The tuning of only 7 channels in the short cavity is observed, which can be explained by the fact that average gain spectrum shifts to shorter wavelength due to gain contribution or loss reduction in the passive section [8]. When the tuning current is further increased above 30 mA, the carrier injection effect tends to saturate and the thermal effect starts to play the dominant role which tunes the channels to shorter wavelength. According to the Vernier principle, when the tuning current is injected into the long cavity of VCL, the carrier injection effect shifts the lasing channel to shorter wavelength. When the tuning current is injected into the short cavity of the VCL, the lasing channel shifts in the opposite direction. Also, this tuning current is much lower than that of all-active VCL. The side mode suppression ratio (SMSR) of the channels are all above 35 db. Fig. 5 gives an example lasing spectrum showing the SMSR of 41.3 dB. Compared to multi-electrode controlled tunable lasers, such as SG-DBR laser, DS-DBR laser, and MG-Y laser, the single-electrode tuned algorithm is much simpler and the drive circuit is easier to realize.

By varying the current injected into the long cavity electrode and the TEC temperature, 32-channel consecutive wavelength tuning of about 100 GHz is obtained. Fig. 6 shows the overlapped emission spectra of 32 channels and the tuning curves under 3 TEC temperatures are further detailed. The mechanism of the temperature-induced tuning range extension has been discussed in [7]. The large tuning range covers from 1528.78 nm to 1552 nm. Due to the fluctuation of the chip to fiber coupling efficiency during the test, the peak power of the spectrum varies slightly from channel to channel, which can be reduced by the module package.
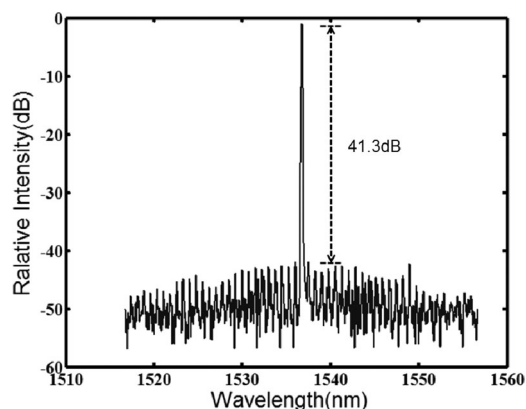
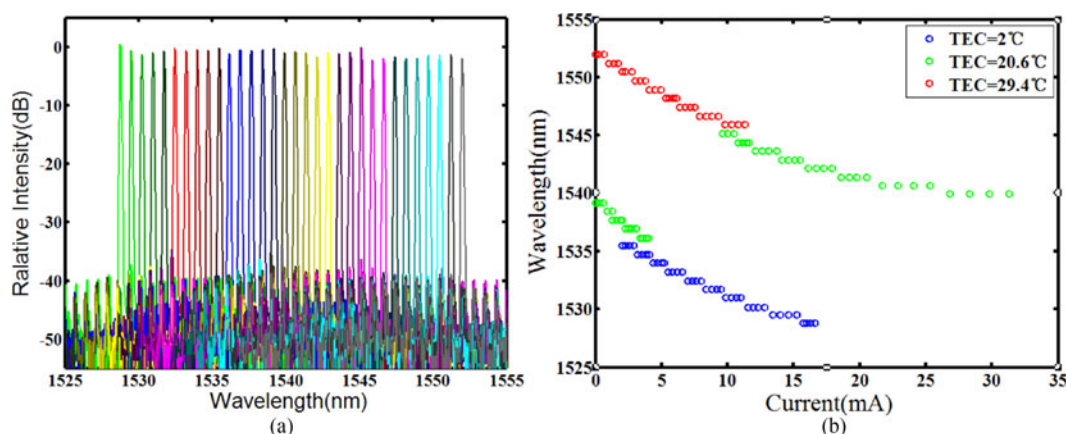Fig. 5. Single mode emission spectrum of VCL with 41.3 dB SMSR.

Fig. 6. (a) Measured superimposed 32-channel spectra and (b) the tuning curves.

In the applications such as packet-based wavelength routing, the switching speed is an important parameter. Less than 30 ns switching time is required. This can be achieved in the VCL with butt-joint passive tuning section using the free carrier plasma effect. To demonstrate this, a square wave signal (frequency = 39 MHz, duty cycle = 0.5, rise/fall time T0 = 133 ps) is applied on the long-cavity electrode. After amplification by an optical amplifier, the light passes through a tunable narrow-bandwidth filter to select a target wavelength channel and an optical oscilloscope to display the switching transient waveform. The profile of the filter is Gaussian-type and the 3 dB bandwidth is set to 0.4 nm. The injected currents on the gain electrode and the short cavity electrode are kept constant at 150 and 0 mA, respectively. Fig. 7 show the switching transient response for switching between adjacent modes (a) and nonadjacent modes (b), respectively.

In the case of adjacent mode switching, when the injection current is biased at 1.4 mA and the peak-peak current modulation is set at 0.3 mA, mode jumps back and forth between 1538.00 nm and 1538.78 nm without exciting any other modes. The channel switching delays, which are defined as the delay from the time when the power of the turn-off channel is decreased to 90% of the maximum to the time when the power of the turn-on channel is increased to 90% of the maximum, are around 1.8 ns for adjacent modes. In the case of nonadjacent mode switching, when the injection current is biased at 2.4 mA and the peak-peak current modulation is set at 2 mA, which correspond to current change from mode A (1536.50 nm) to mode D (1538.78 nm), mode B (1537.26 nm) and mode C (1538.00 nm) can be observed during the transient time. When the wavelength is switched from 1538.78 nm to 1536.5 nm, the 1537.26 nm is close to the destination channel with the stronger signal than 1538.00 nm. Also when the wavelength is switched back,
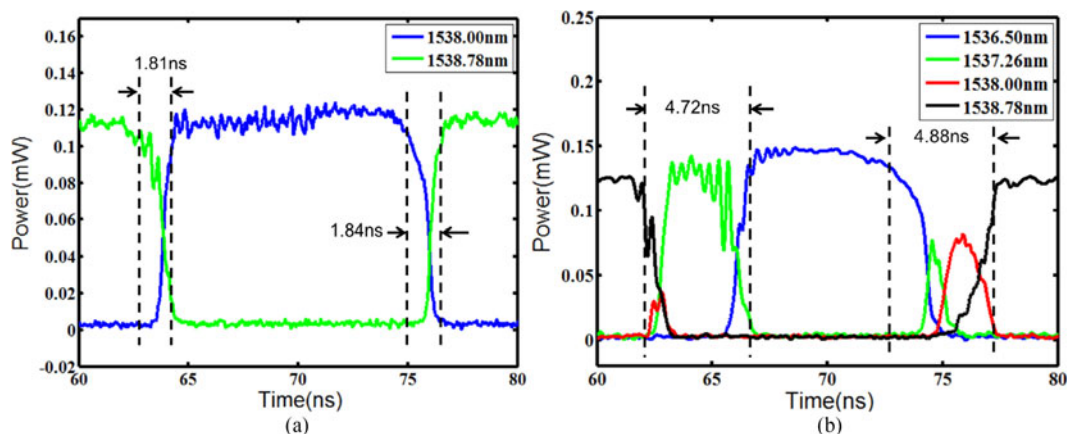
Fig. 7. Wavelength switching waveforms between (a) adjacent modes and (b) nonadjacent modes.
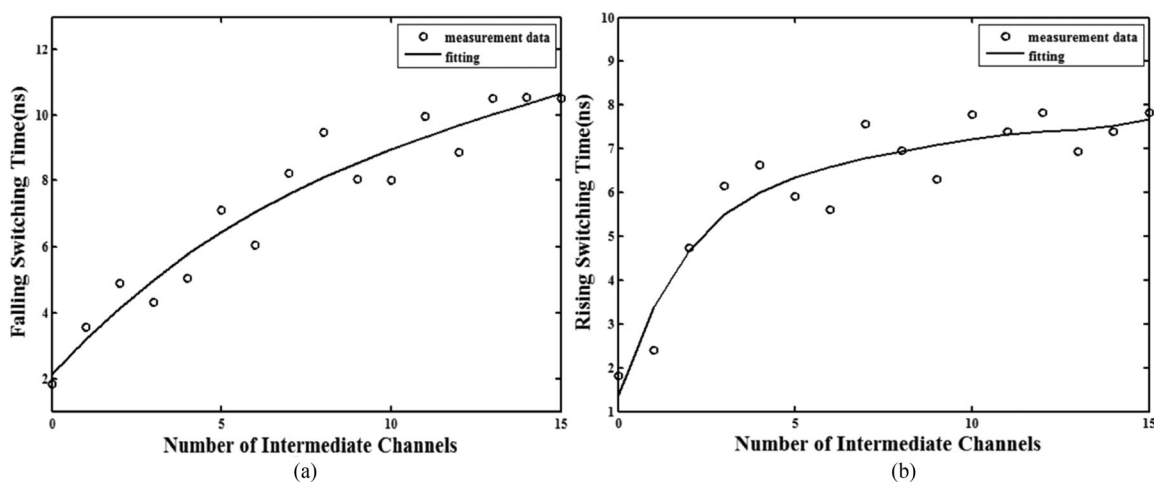

Fig. 8. (a) The rise and (b) fall times of the wavelength switching versus the number of intermediate channels.

the mode C at 1538.00 nm is close to the destination channel with the stronger signal than the mode B at 1537.26 nm.The spikes in the curves of mode A and D are caused by the optical power variation during the switching transient. Thus the switching forward and backward delays time for the destination channel are 4.72 and 4.88 ns, respectively.

Though the wavelength tuning is realized by current induced index change, the thermal effects induced by current injection during the tuning cannot be avoided. However, when the carrier injection effect dominates the wavelength switching, the injected current is typically below 40 mA, thus the refractive index change by the thermal effects is small. Moreover, due to the discrete channel tuning characteristics as shown in Fig. 4, the wavelength variation is very small within a channel (flat horizontal lines). Thus the refractive index change by thermal effect affects the wavelength very little. The thermal stabilization time is therefore not important.

The rise and fall times of the wavelength switching between two channels are plotted in Fig. 8 as a function of the number of intermediate channels. The switching time generally increases with the number of intermediate channels. However, the increase of the rise and fall times saturates at 8 ns and 11 ns, respectively. The fall time of the wavelength switching from the lower current mode (1538.78 nm) to the higher current mode (1538.00 nm or 1544.86 nm) is a little shorter than the rise time of the wavelength switching in the opposite direction. This can be explained by the fact that the carrier density falls slightly slower than it rises. The switching time is a little shorter than

that based on QWI platform (12 ns) [8] and is over 3 orders of magnitude faster than that based on electro-thermal-optical effect (20 μs) with all active structure [7].

4. Conclusion

In conclusion, we have designed and fabricated a widely tunable V-coupler laser, in which the active MQW laser structure is butt-jointed with the passive tuning section. Using the carrier plasma based tuning effect, over 25-nm wavelength tuning with 100 GHz channel spacing is obtained. A larger tuning range can be achieved by reducing the cavity length difference at the expense of lower SMSR. The switching delay time varies from 1 to 11 ns, depending on the interval between the switching channels. The single electrode controlled fast wavelength switching between ITU channels has great potential in future wavelength routed optical networks.

Reference

[1] S. J. Park, C. H. Lee, K. T. Jeong, H. J. Park, J. G. Ahn, and K. H. Song, "Fiber-to-the-home services based on wavelength-division-multiplexing passive optical network," *J. Lightw. Technol.*, vol. 22, no. 11, pp. 2582–2591, Nov. 2004.
[2] A. Banerjee *et al.*, "Wavelength-division-multiplexed passive optical network (WDM-PON) technologies for broadband access: A review," *J. Opt. Netw.*, vol. 4, no. 11, pp. 737–758, Nov. 2005.
[3] J. Jin, L. Wang, T. Yu, Y. Wang, and J. J. He, "Widely wavelength switchable V-coupled-cavity semiconductor laser with ~40 dB side-mode suppression ratio," *Opt. Lett.*, vol. 36, no. 21, pp. 4230–4232, Nov. 2011.
[4] J. J. He and D. Liu, "Wavelength switchable semiconductor laser using half-wave V-coupled cavities," *Opt. Exp.*, vol. 16, no. 6, pp. 3896–3911, Mar. 2008.
[5] J. W. Raring *et al.*, "40Gb/s widely tunable low-drive-voltage electroabsorption-modulated transmitters," *J. Lightw. Technol.*, vol. 25, no. 1, pp. 239–248, Jan. 2007.
[6] J. E. Johnson *et al.*, "10 Gb/s transmission using an electroabsorption-modulated distributed Bragg reflector laser with integrated semiconductor optical amplifier," in *Proc. Opt. Fiber Commun. Conf. Exhibit,* 2001, Paper TuB3.
[7] S. Zhang, J. Meng, S. Guo, L. Wang, and J. J. He, "Simple and compact V-cavity semiconductor laser with 50 × 100 GHz wavelength tuning," *Opt. Exp.*, vol. 21, no. 11, pp. 13564–13571, Jun. 2013.
[8] X. Zhang, J. J. He, N. Liu, and J. J. Dubowski, "Carrier-induced fast wavelength switching in tunable V-cavity laser with quantum well intermixed tuning section," *Opt. Exp.*, vol. 23, no. 20, pp. 26336–26341, Sep. 2015.
[9] Y. Barbarin *et al.*, "Buttjoint interfaces in InP/InGaAsP waveguides with very low reflectivity and low loss," *Clin. Cancer Res.*, vol. 11, no. 1, pp. 79–86, Aug. 2005.
[10] X. Liao, J. Meng, and J. J. He, "Tunable V-coupled-cavity semiconductor laser monolithically integrated with monitoring photodiodes using deeply etched reflective trenches," *Proc. SPIE*, vol. 9267, Dec. 2014, Art. no. 926715.
[11] X. Lin, D. Liu, and J. J. He, "Design and analysis of 2 × 2 half-wave waveguide couplers," *Appl. Opt.*, vol. 48, no. 25, pp. F18–F23, May 2009.
[12] T. L. Koch and U. Koren, "Semiconductor lasers for coherent optical fiber communications," *J. Lightw. Technol.*, vol. 8, no. 3, pp. 274–293, Mar. 1990.
[13] S. Liang, L. Han, L. Qiao, J. Xu, H. Zhu, and W. Wang, "DBR laser with over 20 nm wavelength tuning range," *IEEE Photon. Technol. Lett.*, vol. 28, no. 9, pp. 943–946, May 2016.
[14] F. Rana, C. Manolatou, and M. F. Schubert, "Tapered cavities for high-modulation-efficiency and low-distortion semiconductor lasers," *IEEE J. Quantum Electron.*, vol. 43, no. 11, pp. 1083–1087, Nov. 2007.
[15] J. J. He and D. Liu, "Wavelength switchable semiconductor laser using half-wave V-coupled cavities," *Opt. Exp.*, vol. 16, no. 6, pp. 3896–3911, Mar. 2008.